

1 **Synchronous emplacement of the anorthosite
2 xenolith-bearing Beaver River diabase and one of the
3 largest lava flows on Earth**

4 **Yiming Zhang¹, Nicholas L. Swanson-Hysell¹, Mark D. Schmitz², James D.
5 Miller Jr.³, Margaret S. Avery^{1,4}**

6 ¹Department of Earth and Planetary Science, University of California, Berkeley, CA, USA

7 ²Department of Geosciences, Boise State University, Boise, ID, USA

8 ³Department of Earth and Environmental Sciences, University of Minnesota, Duluth, MN, USA

9 ⁴Geology, Minerals, Energy, and Geophysics Science Center, U.S. Geological Survey, Moffett Field, CA,
10 USA

11 **Key Points:**

- 12 • New geochronology on an anorthosite xenolith tightly constrain the timing of the
13 Beaver River diabase intrusions.
- 14 • Paleomagnetic and geochronological data support that the Beaver River diabase
15 is comagmatic with the very high volume Greenstone Flow.
- 16 • Wide conduits of magma to the surface are indicated by large anorthosite xeno-
17 liths.

Corresponding author: Yiming Zhang, yimingzhang@berkeley.edu

18 **Abstract**

19 New geochronologic and paleomagnetic data from the North American Midcontinent Rift
 20 (MCR) reveal the synchronous emplacement of the Beaver River diabase, the anorthosite
 21 xenoliths within it, and the Greenstone Flow — one of the largest lava flows on Earth.
 22 A U-Pb zircon date of 1091.83 ± 0.21 Ma (2σ) from one of the anorthosite xenoliths is
 23 consistent with the anorthosite cumulate forming as part of the Midcontinent Rift and
 24 provides a maximum age constraint for the Beaver River diabase. Paired with the min-
 25 imum age constraint of a cross-cutting Silver Bay intrusion (1091.61 ± 0.14 Ma; 2σ) these
 26 data tightly bracket the age of the Beaver River diabase to be 1091.7 ± 0.2 Ma (95% CI),
 27 coeval with the eruption of the Greenstone Flow — which is further supported by in-
 28 distinguishable tilt-corrected paleomagnetic pole positions. These data, as well as min-
 29 eralogical and geochemical data, support the hypothesis that the Beaver River diabase
 30 that entrained large anorthosite xenoliths was the feeder system for the Greenstone Flow.
 31 The large areal extent of the intrusives and large estimated volume of the volcanics sug-
 32 gest that they represent a rapid and voluminous *ca.* 1092 Ma magmatic pulse near the
 33 end of the main stage of MCR magmatism.

34 **1 Introduction**

35 The North American Midcontinent Rift (MCR) is a *ca.* 1.1 Ga large igneous province
 36 for which there is excellent exposure of both the intrusive and extrusive components in
 37 the Lake Superior region (Fig. 1). An exceptional feature of the Midcontinent Rift is the
 38 occurrence of large anorthosite xenoliths (whose diameter can exceed 150 meters) within
 39 a diabase sill and dike network known as the Beaver River diabase that outcrops in north-
 40 eastern Minnesota, USA, as part of the Beaver Bay Complex (Fig. 1). Despite these anorthosite
 41 xenoliths having long been recognized and mapped, the origin of these nearly pure pla-
 42 gioclase cumulates has been debated in the literature (Lawson, 1893; Grout, 1939; Mor-
 43 rison et al., 1983; Miller & Chandler, 1997). Lacking the roadcut exposures that now make
 44 the xenolithic relationship clear and observing the large blocks exposed along the Lake
 45 Superior shoreline and at Carlton Peak, Lawson (1893) did not recognize the anorthosites
 46 as xenoliths. Rather, he argued that the anorthosite is Archean in age and that the Ke-
 47 weenawan (i.e. Midcontinent Rift related) magma was emplaced atop an anorthosite ero-
 48 sional unconformity surface. Later work established the anorthosite blocks as xenoliths,
 49 which are now extensively documented through geologic mapping of the region (Fig. 1;

50 Miller et al. (2001); Miller (1988); Miller and Boerboom (1989); Boerboom (2004); Boer-
51 boom and Green (2006); Boerboom et al. (2006, 2007)) and outcrop-scale exposures (Fig.
52 3).

53 The anorthosite xenoliths range in size from centimeter-scale megacrysts to meter-
54 scale, decimeter-scale and even >150 meter-scale blocks (Fig. 3; Morrison et al. (1983);
55 Grout (1939)). There have been divergent interpretations regarding the age and magma
56 source of these anorthosite xenoliths (Fig. 1). Grout (1939) recognized the xenolithic na-
57 ture of the anorthosites and suggested that the massive intrusion of the older anorthositic
58 gabbro within the Duluth Complex may have supplied anorthosite fragments that were
59 later entrained by the Beaver River diabase emplacement. However, the distinctive modes,
60 textures, mineral chemistry, and trace element and isotopic (Sm-Nd, Rb-Sr) composi-
61 tions between the anorthosite xenoliths and the *ca.* 1096 Ma Anorthositic Series of the
62 Duluth Complex challenge this interpretation. Morrison et al. (1983), on the other hand,
63 argued that the xenoliths were sourced from Paleoproterozoic or Archean lower crust that
64 were liberated and contaminated by Midcontinent Rift magmas based on Sm and Nd iso-
65 topic data. They interpreted a Sm-Nd model age of 1.9 Ga from one of the xenoliths as
66 providing a minimum crystallization age for the anorthosites though they acknowledged
67 that these constraints are not definitive with respect to the age.

68 In contrast to this Archean to Paleoproterozoic model, Miller and Chandler (1997)
69 favored a scenario where the anorthosite crystallized as part of Midcontinent Rift mag-
70 matism. They cited work by Kushiro (1980) who showed that the changing density con-
71 trast between labradoritic to bytownitic plagioclase and tholeiitic magma at different crustal
72 pressures would promote flotation of plagioclase in deep (>20 km) crustal magma cham-
73 bers and the creation of anorthosite cumulates in the lower crust. This mechanism of
74 plagioclase flotation likely created massive anorthosite cumulates in the roof zones of sub-
75 crustal magma chambers during MCR magmatism. Miller and Weiblen (1990) specu-
76 lated that plagioclase-phyric magmas tapped from these deep chambers fed shallow (~5km)
77 subvolcanic intrusions of the Duluth Complex, thereby creating the anorthositic gabbros
78 of the Anorthositic Series. Miller and Chandler (1997) suggested that the nearly pure
79 anorthosite xenoliths occurring in the younger and more hypabyssal diabase intrusions
80 of the Beaver Bay Complex were harvested from these phase-segregated intrusions in the
81 lower crust. They further argued that the isotopic data of Morrison et al. (1983) can be
82 explained by anorthosite-forming MCR magmas having been contaminated by older crust

83 rather than the anorthosites being older lower crust that was contaminated by MCR mag-
84 mas.

85 Regardless of their origin, the exceptional sizes of some of the anorthosite xeno-
86 liths reveal the immense widths of the Beaver River diabase conduits. A particularly large
87 anorthosite xenolith is exposed at Carlton Peak in the eastern Beaver Bay Complex with
88 minimum dimensions of 180×240 meters (Fig. 1, 3; Boerboom et al. (2006)). In the
89 southern Beaver Bay Complex, a large anorthosite xenolith near Corundum Point has
90 dimensions of 180×230 meters while the one exposed at Split Rock Point has dimen-
91 sions of 180×260 meters (Boerboom, 2004). To be able to accommodate such large xeno-
92 liths during magma ascent from the lower crust, the Beaver River diabase conduits must
93 have been of at least the width of the anorthosite short axis diameters. Such wide con-
94 ducts in these near-surface intrusions suggest high magma flux rates and make it likely
95 that the magma extruded to the surface — feeding voluminous lava flows.

96 Miller and Chandler (1997) emphasized the composite nature of the Beaver River
97 diabase network and Silver Bay intrusions (Fig. 1), which are locally marked by abrupt
98 transitions to progressively more evolved lithologies. Furthermore, that study documented
99 geochronologic, geochemical and structural evidence to support the notion that the di-
100 abase network may have served as principal feeder conduits to lava flows including parts
101 of the Portage Lake Volcanics on the Keweenaw Peninsula and Isle Royale of Michigan
102 (Fig. 1). To more directly test this inferred intrusive-extrusive correlation, Doyle (2016)
103 compared the mineralogical, textural, and geochemical attributes and the composite litho-
104 logic nature of the Beaver River diabase against those of the Greenstone Flow, the largest
105 lava flow within the Midcontinent Rift and one of the largest lava flows on Earth (Fig.
106 2). The Greenstone Flow also has a composite nature, which is indicated by its litho-
107 logic zonation of ophitic basalt forming the upper and lower zones and an interior zone
108 composed of prismatic ferrogabbro to granophyric monzodiorite. Doyle (2016) documented
109 remarkable similarities in petrography, mineral chemistry, whole rock geochemistry, and
110 lithologic zonation between the Beaver River diabase intrusions in northern Minnesota
111 and the Greenstone Flow on both Isle Royale and Keweenaw Peninsula. Based on the
112 interpreted feeder system being in northern Minnesota, Doyle (2016) estimated the full
113 extent of the Greenstone Flow to be ~ 20000 km 2 and its volume to be between 2000 and
114 6000 km 3 (Fig. 2).

A comagmatic relationship between the Beaver River diabase and the Greenstone Flow is consistent with the similar $^{207}\text{Pb}/^{206}\text{Pb}$ dates developed from a granophyric ferrogabbro within the Beaver Bay Complex (1095.8 ± 1.2 Ma, Paces and Miller (1993)) and the Greenstone Flow (1094.0 ± 1.5 Ma, Davis and Paces (1990)). The relatively large uncertainties provided by the existing $^{207}\text{Pb}/^{206}\text{Pb}$ geochronology more roughly constrains the temporal relationships between these rapid events than is possible with modern methods. Modern-day U-Pb geochronology techniques for chemical abrasion isotope dilution-thermal ionization mass spectrometry (CA-ID-TIMS) allow high precision $^{206}\text{Pb}/^{238}\text{U}$ dates to be developed from chemically-abraded zircon crystals (Mattinson, 2005). Studies utilizing these methods on Midcontinent Rift volcanics and intrusions have shown that the analytical uncertainties on weighted mean $^{206}\text{Pb}/^{238}\text{U}$ dates of multiple chemically-abraded single zircons can be of ~ 200 kyr, an order of magnitude smaller than previous dates that are based exclusively on the $^{207}\text{Pb}/^{206}\text{Pb}$ system (Fairchild et al., 2017; Swanson-Hysell et al., 2019, 2020). These $^{206}\text{Pb}/^{238}\text{U}$ dates are also considered to be more accurate than systematically older $^{207}\text{Pb}/^{206}\text{Pb}$ dates (Schoene et al., 2006). Such $^{238}\text{U}/^{206}\text{Pb}$ dates have revealed that the massive Layered Series and Anorthositic Series rocks of the Duluth Complex were emplaced in ~ 500 kyr *ca.* 1096 Ma (Swanson-Hysell et al., 2020).

In this work, we use a new $^{206}\text{Pb}/^{238}\text{U}$ zircon date for an anorthosite xenolith within the Beaver River diabase, in conjunction with $^{206}\text{Pb}/^{238}\text{U}$ dates from a Silver Bay intrusion and the Greenstone Flow (Fig. 1; Fairchild et al. (2017)), to evaluate the timing of emplacement of the Beaver River diabase, and the hypothesized intrusive-extrusive correlation between the Beaver River diabase and the Greenstone Flow.

Paleomagnetic data can also provide chronological constraints on rock units. Laurentia experienced a period of rapid latitudinal plate motion during rift development (Swanson-Hysell et al., 2009). A synthesized apparent polar wander path (APWP) based on the Midcontinent Rift volcanic rocks indicates that motion exceeded 20 cm/yr (Swanson-Hysell et al., 2019), faster than the maximum speed of India of ~ 17 cm/yr during the Cenozoic (van Hinsbergen et al., 2011). This motion resulted in significant differences in pole positions recorded by Midcontinent Rift rocks that were emplaced a few million years apart (Swanson-Hysell et al., 2019). In this study, we present paleomagnetic data from the anorthosite xenoliths and the host Beaver River diabase. Data from the xenoliths give equivalent directions to the host diabase (Figs. 5, 6), indicating that they were heated above the Curie temperature of magnetite and acquired a thermal remanent mag-

netization when they cooled within the diabase. This thermal history is consistent with thermal diffusion modeling of the xenoliths (Fig. ??). The paleomagnetic data can be compared to data from the Greenstone Flow to further test the hypothesis that they are synchronous. The resulting paleomagnetic pole positions can also be compared to the synthesized Laurentia APWP to obtain chronological constraints (Fig. 6).

Here, by integrating the geochronologic and paleomagnetic perspectives with previous lithologic and geochemical analyses (Miller & Chandler, 1997; Doyle, 2016), we more definitely establish that the Beaver River diabase network acted as the feeder system for the Greenstone Flow of the Portage lake Volcanic-equivalent flows. Their shared geochemical signatures, composite nature of emplacement, and the inference of giant magma conduits that transported large anorthositic xenoliths characterize a period of *ca.* 1092 Ma voluminous magmatic activity (based on $^{206}\text{Pb}/^{238}\text{U}$ zircon dates; Fig. 1).

2 Geologic Setting

2.1 Beaver Bay Complex and Related Rocks of NE Minnesota

The North American Midcontinent Rift (MCR) is a failed intracontinental rift where protracted magmatic activity lasted from *ca.* 1109 Ma to *ca.* 1084 Ma (Swanson-Hysell et al., 2019). Midcontinent Rift rocks extensively outcrop in today's Lake Superior region, with the total extent traceable by arcuate magnetic and gravity anomalies that extend to the southwest to Kansas, and to the southeast, to southern Michigan (Hinze & Chandler, 2020). Previous studies have divided magmatic activity in the rift into four stages based on interpreted changes in relative magmatic volume and the nature of magmatism: early (\sim 1109–1104 Ma), latent (\sim 1104–1098 Ma), main (\sim 1098–1090 Ma) and late (\sim 1090–1083 Ma) (Vervoort et al., 2007; Heaman et al., 2007; Miller & Nicholson, 2013). In northeastern Minnesota, the Early Gabbro Series and the Felsic Series rocks of the Duluth Complex and reversed-polarity lavas of the lower North Shore Volcanic Group were emplaced during the early stage. The more voluminous Duluth Complex Layered Series and the plagioclase-rich Anorthositic Series, together with an associated \sim 8 km thick extrusive volcanic sequences of the North Shore Volcanic Group (NSVG), were rapidly emplaced about 10 myr later at *ca.* 1096 Ma during the main stage (Paces & Miller, 1993; Swanson-Hysell et al., 2020).

The Beaver Bay Complex, which sits stratigraphically above the Duluth Complex, is another intrusive complex that resulted from main stage magmatism. The exposed area of the Beaver Bay Complex is $\sim 1000 \text{ km}^2$ where it has been mapped along the north-western shore of Lake Superior in northeastern Minnesota (Fig. 1; Supporting Information). The Beaver Bay Complex is a multi-phase, composite intrusive complex that intrudes parts of the NSVG (Fig. 1; Miller and Chandler (1997); Swanson-Hysell et al. (2020)). Distinct from the deep plutonic intrusions of the Duluth Complex, the majority of the Beaver Bay Complex is formed of hypabyssal intrusions that were emplaced as dikes and sills at shallow depths (Miller & Chandler, 1997). Detailed mapping and petrological analyses of the Beaver Bay Complex have led to the identification of thirteen intrusive units and at least six major intrusive events (Miller & Chandler, 1997). Most of the Beaver Bay Complex intrusions are dioritic to gabbroic in composition (Miller & Chandler, 1997). The main lithology of the Beaver River diabase dikes and sills network within the Beaver Bay Complex is an ophitic olivine gabbro (Fig. 3), but in wider areas of dikes and the upper parts of thick sills, this rock type can abruptly transition into intergranular olivine oxide gabbro, then to subprismatic (and commonly foliated) ferrogabbro, and finally to granophyric monzodiorite. The more evolved and later emplaced components of the Beaver River diabase network are commonly distinguished as the Silver Bay intrusions in the southern Beaver Bay Complex (Fig. 1). Overall being intermediate in composition, the Silver Bay intrusions lithologies range from ophitic olivine gabbro to ferrogranite (Shank, 1989). Field mapping by Miller et al. (1994) found intrusive relationship between the Silver Bay intrusions and the Beaver River diabase. Angular inclusions of the host Beaver River diabase within marginal zones of the Silver Bay intrusions led Miller and Chandler (1997) to interpret that the Silver Bay intrusions intruded after the diabase crystallized.

One distinctive feature of the Beaver River diabase is its inclusions of anorthosite xenoliths. In the southern part of the Beaver Bay Complex, the Beaver River diabase occurs as dikes and sills, typically including anorthosites with various sizes ranging from centimeters to over 150 meters (Figs. 1, 3; Grout (1939); Morrison et al. (1983)). The diabase in this region intrudes the Palisade rhyolite of the North Shore Volcanic Group (Fig. 1), which has a $^{206}\text{Pb}/^{238}\text{U}$ date of $1093.94 \pm 0.28 \text{ Ma}$ (2σ analytical uncertainty is presented for CA-ID-TIMS dates throughout this work; (Swanson-Hysell et al., 2019)). The Beaver River diabase is locally intruded by the Silver Bay intrusions (Fig. 1). An

211 aplite unit within the granophyre zone of one of these Silver Bay intrusions has a $^{206}\text{Pb}/^{238}\text{U}$
212 date of 1091.61 ± 0.14 Ma (Swanson-Hysell et al., 2019). Another arcuate, sill-like di-
213 abase body mapped as the Beaver River diabase outcrops along the eastern part of the
214 complex (Fig. 1; Miller and Chandler (1997)). The diabase composition there is simi-
215 lar to that in the south and it also contains large anorthosite xenoliths that exceed 100
216 meters at Carlton Peak (Fig. 1). The Beaver River diabase in the northern part of the
217 complex near the Houghtaling Creek area typically forms narrow, near-vertical dikes in-
218 stead of sheets in the southern and eastern regions (Fig. 1; Miller et al. (1994)). The di-
219 abase in this region only locally contains xenoliths of anorthosite at dike margins.

220 Hundreds of anorthosite xenoliths have been recognized and mapped within the
221 Beaver River diabase (Fig. 1). Many hill tops in the Beaver Bay Complex, such as the
222 Carlton Peak and Britton Peak, are large anorthosite blocks (which lead Lawson (1893)
223 to erroneously conclude that they were relict Archean topography). In the field, the anorthosites
224 typically appear as subrounded to rounded, light-colored, translucent blocks that are in
225 sharp contact with the hosting diabase (Fig. 3). They also occur as exposures whose con-
226 tact with the diabase is covered (Fig. 3). Grout (1939) suggested that the rounded anorthosites
227 are the result of friction during transportation as they were liberated by the diabase (i.e.
228 physical weathering within a magmatic system). While the Beaver River diabase is chilled
229 against the North Shore Volcanic Group lithologies that it intrudes, the diabase is not
230 chilled against the margin of the anorthosite xenoliths (Morrison et al., 1983; Miller &
231 Chandler, 1997). The lack of chilled contacts is consistent with the anorthosite being at
232 elevated temperatures and cooling at the same time as the diabase magma (Fig. 7).

233 The anorthosite xenoliths are dominantly monomineralic plagioclase that has an
234 average anorthite content of $\sim 70\%$ (Morrison et al., 1983; Doyle, 2016). Interstitial py-
235 roxene and olivine are present in minor concentrations in the xenoliths. Within the Carl-
236 ton Peak anorthosite xenolith, up to 10 cm oikocrysts of altered mafic minerals such as
237 olivine can occur. Nevertheless, the overall olivine content in the anorthosites is low. In-
238 terstitial titanomagnetite-ilmenite intergrowths that exceed $100 \mu\text{m}$ can be found through
239 microscopy and $<20 \mu\text{m}$ Fe-Ti oxide grains can be detected with scanning electron mi-
240 croscopy (Fig. 3). Based on textural differences Morrison et al. (1983) divided the anorthosite
241 xenoliths into four groups: one group which typically have well-developed granoblastic
242 texture characterized by equigranular plagioclase crystals; another group which have in-
243 terlocking, lath-shaped plagioclase crystals; an intermediate group which can have both

244 granoblastic texture and interlocking plagioclase laths; and a brecciated group that have
 245 brittle deformation textures superposed on pre-existing textures.

246 2.2 Portage Lake Volcanics and the Greenstone Flow

247 The Portage Lake Volcanics (PLV) is a ~5 km thick, normally magnetized, dom-
 248 inantly olivine basalt to andesite volcanic succession that outcrops in northern Michi-
 249 gan (particularly along the Keweenaw Peninsula) as well as on Isle Royale (Fig. 1, Huber
 250 (1973); Cannon and Nicholson (2001); Green (1982)). The Greenstone Flow of the Portage
 251 Lake Volcanic Group has been recognized as one of the largest lava flows on earth (Figs.
 252 1, 2). It outcrops as the main ridge along the Keweenaw Peninsula and Isle Royale (Fig.
 253 1). The flow can be correlated between the two outcrop regions on the basis of geochem-
 254 ical, petrographic, and paleomagnetic similarity of the flow itself and the flows above and
 255 below (Longo, 1984). In both outcrop regions, the Greenstone Flow is underlain by con-
 256 glomerate and overlain by pyroclastic breccia (Lane, 1911; Huber, 1973). On the Keweenaw
 257 Peninsula, the Greenstone Flow is exposed over 90 km with a range of thickness from
 258 ~100 meters to a maximum thickness of over 450 meters, dipping to the northwest (Fig.
 259 1; White (1960)). On Isle Royale, the Greenstone Flow has a range of thickness from ~30
 260 meters to a maximum thickness of about 250 meters, dipping toward the southeast (Fig.
 261 1; Huber (1973)). More recently, Doyle (2016) estimated that the total aerial extent of
 262 the Greenstone Flow could be up to ~20000 km². Taking a range for this thickness of
 263 100 to 300 meters, Doyle (2016) estimated a total volume of 2000 to 6000 km³. This vol-
 264 ume range makes the Greenstone Flow one of the largest, if not the largest, single mafic
 265 lava flows on Earth (Fig. 2).

266 According to mineralogical and textural attributes, Doyle (2016) divided the Green-
 267 stone Flow into four zones from bottom to top — lower ophitic zone, heterolithic zone,
 268 upper ophitic zone, and an amygdaloidal zone. Field observations, geochemical analy-
 269 ses and parent magma calculations conducted by Doyle (2016) suggest that the zoned
 270 Greenstone Flow formed through an open-system differentiation of a composite parent
 271 magma which is more evolved than the primitive olivine tholeiites generated by the Mid-
 272 continent Rift plume. That study proposed that the emplacement of the Greenstone Flow
 273 started with a voluminous eruption of olivine tholeiitic magma, forming the ophitic zones
 274 which subsequently inflated due to composite intrusions of more evolved basaltic magma
 275 which composes the heterolithic zone. A final stage of localized melt migration and dif-

276 differentiation resulted in the heterogeneous composition of the heterolithic zone. A $^{206}\text{Pb}/^{238}\text{U}$
 277 zircon date of 1091.59 ± 0.27 Ma for the Greenstone Flow was developed from a peg-
 278 matoid sample from the heterolithic zone (Swanson-Hysell et al., 2019).

279 3 Methods and Results

280 3.1 Zircon Geochronology and Geochemistry

281 A sample of an anorthosite xenolith within the Beaver River diabase was collected
 282 for U-Pb geochronology along Hwy 61 across from the Silver Bay taconite plant (MS99033;
 283 91.26358°W 47.28888°N ; Fig. 1). This sample comes from the same xenolith sampled for
 284 paleomagnetic study as site AX16 which has an exposed diameter of 27.5 meters (Fig.
 285 3). Thin sections were made from the geochronology sample as well as multiple paleo-
 286 magnetic cores. As is shown in Fig. 3F, plagioclase in this anorthosite xenolith have both
 287 equigranular crystals displaying a granoblastic texture and lath-shaped crystals display-
 288 ing an interlocking texture. The occurrence of both textures is consistent with an inter-
 289 pretation that this anorthosite xenolith formed under elevated temperatures and expe-
 290 rienced heating after initial crystallization.

291 Zircons were separated from a kilogram of the anorthosite using common mineral
 292 separation methods (Supporting Information). The separated zircons were subhedral to
 293 anhedral crystals (z1-z4) and platy fragments (z5-z8). The subhedral to anhedral crys-
 294 tals are consistent with intercumulus crystallization within an adcumulate with platy frag-
 295 ments also being a common zircon morphology within the Duluth Complex anorthositic
 296 series (e.g. samples AS-1 and FC-1 of Paces and Miller (1993)). Eight chemically-abraded
 297 zircons were analyzed by isotope dilution-thermal ionization mass spectrometry (ID-TIMS)
 298 in the Boise State Isotope Geology Laboratory using EARTHTIME tracer solutions (Condon
 299 et al., 2015). Both zircon morphologies yield indistinguishable dates. Using six of these
 300 single grain dates (and excluding two due to interpreted Pb-loss) results in a weighted
 301 mean $^{206}\text{Pb}/^{238}\text{U}$ date of $1091.83 \pm 0.21/0.37/1.15$ Ma (analytical/ analytical+tracer/
 302 analytical+tracer+decay uncertainty; Fig. 4).

303 This date provides a tight constraint on the age of the Beaver River diabase. Pre-
 304 viously, the maximum age constraint for the Beaver River diabase came from the rela-
 305 tionship that it cross-cuts the Palisade rhyolite of the North Shore Volcanic Group which
 306 has a $^{206}\text{Pb}/^{238}\text{U}$ date of 1093.94 ± 0.28 Ma (Swanson-Hysell et al., 2019). With this

new date, we know the crystallization age of the diabase to have been near-synchronous or younger than the date from the anorthosite xenolith. The Silver Bay intrusions, from which an aplite has a $^{206}\text{Pb}/^{238}\text{U}$ date of 1091.61 ± 0.14 Ma, (Fairchild et al., 2017), cross-cut the Beaver River diabase. These dates constrain the diabase to have been emplaced between 1091.83 ± 0.21 and 1091.61 ± 0.14 Ma (Fig. 4). Assuming a uniform probability of diabase emplacement between the anorthosite and aplite dates and their normal distributed uncertainties, a 95% confidence interval on the age of the diabase can be estimated by a Monte Carlo simulation (Supporting Information). This analysis gives an age for the diabase of 1091.7 ± 0.2 Ma (95% CI).

Using laser ablation-inductively coupled plasma mass spectrometry (LA-ICPMS), we collected trace element data from 15 additional zircons separated from sample MS90033 with both platy and subhedral to anhedral morphologies. Rare earth elements (REE) analyses from all zircons exhibit a significant chondrite-normalized negative Eu anomaly as opposed to the positive Eu anomaly in plagioclase from anorthosite xenoliths reported by Morrison et al. (1983). This result is consistent with the zircon crystallizing from the interstitial residual melt between the plagioclase crystals in the cumulate. In addition, the Ti-in-zircon thermometer gives a range of estimated zircon crystallization temperatures from 998°C to 860°C with a mean of $\sim 950^\circ\text{C}$ (Ferry and Watson (2007); Supporting Information).

3.2 Paleomagnetism

We sampled standard paleomagnetic cores along the southern and eastern Beaver Bay Complex with a particular focus on acquiring paired sites of anorthosite xenoliths and their local diabase hosts. Sample cores were collected using a hand-held gasoline-powered drill and were oriented using a magnetic compass as well as a sun compass when possible. Sun compass orientations were preferentially used for determining the sample azimuth. Typically, 7-10 cores were drilled for each anorthosite xenolith and their diabase hosts. A total of 17 diabase and 22 anorthosite sites were collected (Table 1). A table that summarizes the measured dimensions of each anorthosite xenolith sampled and the distance between each anorthosite paleomagnetic site and closest diabase host site is provided in the Supporting Information.

337 Samples underwent step-wise demagnetization and analyses in the magnetically shielded
 338 room in the UC Berkeley Paleomagnetism Lab. 7 sites from the Beaver River diabase
 339 underwent alternating field (AF) demagnetization with peak fields from 1 mT to 130 mT.
 340 An ASC TD-48SC thermal demagnetizer was used to demagnetize 10 diabase sites and
 341 all 22 anorthositic sites in a step-wise manner, with reduced step increments between 540°C
 342 and 585°C. The typical magnetic field inside the shielded room is <500 nT and the field
 343 inside the thermal demagnetizer chamber is <10 nT. The quartz glass sample rod of the
 344 UC Berkeley system is typically measured at 5×10^{-12} Am². All remanence measure-
 345 ments were made on a 2G Enterprises DC-SQUID superconducting rock magnetometer
 346 equipped with inline AF coils and an automated sample changer system. The PmagPy
 347 software package was used to implement least-square fits to specimen demagnetization
 348 data (Tauxe et al., 2016). Measurement level data are available within the MagIC database
 349 *for the purposes of review, these data are available in a pre-publication contribution within*
 350 *the MagIC database that can be accessed here: <https://earthref.org/MagIC/17102/400e0fb3-a79b-42bd-aeab-9005d2e3b438>*

352 For both the diabase and anorthositic demagnetization, principal component anal-
 353 yses show that an origin trending characteristic remanent magnetization (ChRM) can
 354 be isolated after the removal of a minimal secondary component during the first few low
 355 coercivity (<10 mT) or low temperature (<200°C) demagnetization steps (Fig. 5). The
 356 ChRMs typically unblock through thermal demagnetization steps from ~500°C to ~580°C,
 357 consistent with them being held by low-titanium titanomagnetite. We interpret this com-
 358 ponent as a primary remanent magnetization acquired during the emplacement and cool-
 359 ing of the Beaver River diabase.

360 The site mean paleomagnetic directions are shown in Table 1. We present both AF
 361 and thermal demagnetization results for the Beaver River diabase as both methods are
 362 effective in removing the secondary components and isolating the coherent and univec-
 363 toral ChRM. Based on specimen and site level demagnetization behavior and the prox-
 364 imity between paired paleomagnetic sites of the anorthositic xenoliths and the diabase,
 365 we grouped the anorthositic xenoliths and their diabase hosts into individual cooling units
 366 and calculated a paleomagnetic pole position as the mean of the cooling unit virtual ge-
 367 omagnetic poles (Fig. 6).

368 Tilt-correcting the paleomagnetic directions to paleohorizontal is necessary for de-
369 veloping accurate paleomagnetic poles from the diabase and the anorthosite xenoliths
370 to be compared to the Keweenawan Track apparent polar wander path (APWP; Fig. 6,
371 Swanson-Hysell et al. (2019)). For intrusive igneous rocks, tilt corrections can be diffi-
372 cult to constrain due to the lack of a clear paleohorizontal reference. Many paleomag-
373 netic studies of Midcontinent Rift intrusive rocks in the Lake Superior region did not ap-
374 ply tilt corrections to their data (e.g., Beck & Lindsley, 1969; Beck, 1970; Books et al.,
375 1966). However, we can determine the structural orientation of the Beaver River diabase
376 using the abundant igneous fabric orientations measured on the diabase as well as bed-
377 ding orientations measured from adjacent volcanic units (Boerboom, 2004; Boerboom
378 & Green, 2006; Boerboom et al., 2006, 2007; Miller et al., 2001). We compile the igneous
379 layering measurements from the Beaver River diabase and the volcanic bedding ori-
380 ntations from the Schroeder-Lutsen basalt which is overlying the Beaver Bay Complex.
381 The mean tilt orientations of both units are similar (diabase dip direction - dip: 128.5
382 - 10.2; basalt dip direction - dip: 142.2 - 13.6). We combine the structural measurements
383 from the Beaver River diabase and the Schroeder-Lutsen basalt and derived two sets of
384 tilt corrections for the paleomagnetic directions of the diabase and anorthosite (dip di-
385 rection - dip in the southern Beaver Bay complex: 128.7 - 12.9; in the eastern Beaver Bay
386 Complex: 145.6-13.1, Supporting Information). The advantage of using the structural
387 orientations from the Schroeder-Lutsen basalt is that the arcuate shape of the Beaver
388 River diabase intrusions is nicely captured by the variation of lava dip directions while
389 the dip angles of the basalt and diabase are very similar (Fig. 1).

390 The tilt-corrected ChRMs in both lithologies are northwest and down, yielding good
391 specimen-level and site-level consistency (Fig. 5, 6). Close directional similarities between
392 each anorthosite xenolith and their host diabase are supported by 9 out of a total of 17
393 diabase-anorthosite paleomagnetic site pairs passing a common mean test (McFadden
394 & McElhinny, 1990). The overall mean directions between the two lithologies are indis-
395 tinguishable as they also pass a common mean test (Fig. 6, McFadden and McElhinny
396 (1990)). For the anorthosite sites that do not pass a common mean test with their di-
397 abase hosts, they nevertheless have coherent specimen-level directions that are close to
398 their host diabase directions (Fig. 6). We also plot the tilt-corrected mean pole of sites
399 from both lithologies (diabase: 32.5°N, 189.5°E, N = 15, A95 = 6.3, k = 37.4; anorthosite:
400 30.9°N, 190.8°E, N = 17, A95: 5.2, k = 48.5) in context of a previously synthesized APWP

401 from the volcanics of the Midcontinent Rift (Swanson-Hysell et al., 2019) and show the
 402 poles to lie near the expected 1090 Ma and 1095 Ma pole positions (Fig. 6). The mean
 403 pole position of the interpreted cooling units (32.7°N , 188.8°E , $N = 15$, $A95 = 5.9$, $k =$
 404 41) lies close to the mean pole position derived from the *ca.* 1092 Ma Portage Lake Vol-
 405 canics (Fig. 6), consistent with the coeval magmatic activity between the Beaver River
 406 diabase and the Portage Lake Volcanics. This cooling unit mean pole paired with the
 407 estimated diabase emplacement age of 1091.7 ± 0.2 Ma is recommended to be used to
 408 as a paleomagnetic pole for the Beaver River diabase in future Laurentia Midcontinent
 409 Rift APWP compilations.

410 3.3 Thermal history model

411 The consistency of the paleomagnetic directions between the anorthosite xenoliths
 412 and the host diabase indicate that the anorthosites were heated above the Curie tem-
 413 perature of low-titanium titanomagnetite ($\sim 580^{\circ}\text{C}$) within the Beaver River diabase. To
 414 determine whether this thermal history is consistent with the geometry of the units and
 415 to gain more insight into the emplacement history of the xenoliths, we developed a cool-
 416 ing model. In this model, the anorthosite xenoliths are considered to be solid spheres
 417 with an initial cool temperature embedded in a uniform sheet of diabase magma (Delaney,
 418 1987; Unsworth & Duarte, 1979). The modeled thermal histories for various sizes of anorthosite
 419 xenoliths are shown in Fig. 7. In one end member case, the initial temperature of the
 420 anorthosites is assumed to be 50°C . While this temperature is unrealistically low given
 421 that the anorthosites likely have a deep crustal source, thermal modeling shows that even
 422 a 100-meter anorthosite xenolith with such low initial temperature would have been heated
 423 to the temperature of the tholeiitic magma (1150°C) within the sill. This temperature
 424 is well above the Curie temperature of magnetite. Anorthosite xenoliths with an assumed
 425 initial temperature of 500°C will equilibrate with the magma temperature on a similar,
 426 but slightly shorter, timescale. Therefore, the model predicts that the remanent mag-
 427 netizations of the anorthosites will be reset during emplacement within the diabase sills,
 428 regardless of their initial temperatures. Model parameters set to match the xenolith AX16,
 429 from which a U-Pb date was developed in this study, leads to a model where the 27.5
 430 m xenolith would have stayed at the magma temperature for about 100 years after sill
 431 emplacement (Fig. 7). This duration estimate is a minimum as it does not consider heat-
 432 ing associated with melt in the lower crust or during ascent prior to emplacement although

433 this was likely rapid. The xenolith would have then cooled through the Curie temper-
 434 ature of magnetite (580°) after ~ 1 kyr and acquired its magnetization as it cooled through
 435 magnetite blocking temperatures (down to $\sim 500^{\circ}$).

436 4 Discussion

437 4.1 Origin and Age of the Anorthosite Xenoliths

438 The anorthosite xenoliths were liberated from depth and emplaced within the shal-
 439 low intrusions of the Beaver River diabase at 1091.7 ± 0.2 Ma (95% CI). This timing
 440 of emplacement is constrained by the Beaver River diabase postdating the new $^{206}\text{Pb}/^{238}\text{U}$
 441 zircon date of 1091.83 ± 0.21 Ma for the AX16 xenolith and being older than the cross-
 442 cutting 1091.61 ± 0.14 Ma Silver Bay intrusives.

443 The most straight-forward interpretation of the U-Pb dates is that the anorthosites
 444 are entrained cumulates that crystallized just before the time of Beaver River
 445 diabase emplacement. This scenario would require that there were large lower crustal
 446 magma chambers in which flotation of plagioclase resulted in cumulate formation both
 447 during *ca.* 1092 Ma Beaver Bay Complex magmatism and *ca.* 1096 Ma Duluth Com-
 448 plex magmatism. We know that during Duluth Complex time, conditions existed for an
 449 anorthosite-generating, deep-crustal magma chamber that resulted in the emplacement
 450 of one of the largest layered mafic intrusions on Earth (Miller & Weiblen, 1990). The
 451 Duluth Complex also contains anorthosite xenoliths within gabbroic anorthosite of the
 452 Anorthositic Series (Fig. 9, Miller and Weiblen (1990)). Both the crystal-rich magma
 453 that formed the Duluth Complex Anorthositic Series and more crystal-poor magmas of
 454 the Duluth Complex Layered Series were rapidly emplaced within < 500 kyr, between
 455 1096.19 ± 0.19 Ma and 1095.69 ± 0.18 Ma ($^{206}\text{Pb}/^{238}\text{U}$ ages, Swanson-Hysell et al. (2020)),
 456 about 4 myr before the emplacement of the Beaver River diabase. Given the known anorthosite
 457 generation during Duluth Complex magmatism, it is worth considering whether it is rec-
 458 oncileable with the data for the anorthosite cumulates xenoliths to have crystallized *ca.*
 459 1096 Ma, but give U-Pb zircon dates of *ca.* 1091.8 Ma.

460 The significant negative Eu anomaly in the zircons within the anorthosite constrains
 461 them to have crystallized from a magma that had experienced significant plagioclase ex-
 462 traction (Rubatto (2002); Schaltegger et al. (1999); Supporting Information). This re-
 463 sult indicates that the zircons were comagmatic with their host anorthosite plagioclase.

The Ti-in-zircon temperature estimates indicate that they crystallized from temperatures of \sim 998 to 860°C (Ferry & Watson, 2007). In addition, zircons that have lower Ti-in-zircon temperatures have lower Eu abundance, but enrichment of incompatible elements such as Hf and Th (Supporting Information). This systematic pattern of elemental concentration variation is consistent with the zircons crystallizing from residual melts on a cooling path that increased incorporation of incompatible trace elements and deepened the Eu anomaly with decreasing temperature and melt fraction. Scanning electron microscopy on two undated anorthosite xenoliths with plagioclase laths displaying interlocking textures reveals zircon crystals with subhedral to anhedral shapes within the mineral assemblage that is interstitial to the plagioclase (Supporting Information). Cathodoluminescence (CL) images show internal zoning in zircons which can be attributed to variations in REE, particularly Dy elemental concentrations, during zircon crystallization (Remond et al. (1992); Supporting Information). These data confirm that the zircons formed from residual melt within the interstitial spaces of the plagioclase cumulate and are inconsistent with a later metamorphic origin.

Zircon U-Pb dates nearly always record crystallization age as the temperatures necessary for significant diffusive Pb loss exceed typical liquidus temperatures of zircon-bearing rocks. However, the anorthosites are a rather unique case given that the melting point of anhydrous plagioclase with an average composition of the Beaver River anorthosite (\sim 70% anorthite, Morrison et al. (1983); Doyle (2016)) is quite high at \sim 1400°C. Thermal history modeling indicates that the xenoliths would have equilibrated to the temperature of the olivine tholeiitic magma (\sim 1100 to 1200°C) and remained at that temperature for more than 100 years in the diabase sill interior (Fig. 7). While these temperatures would not have melted the plagioclase or zircon, these temperatures are high enough for there to start to be appreciable Pb diffusion out of zircon. However, the magnitude of Pb diffusion is dependent on the time spent at such a temperature. If a temperature of 1200°C is sustained for \sim 10 thousand years (longer than the modeled time), \sim 90% of Pb will diffuse out of a \sim 120 μm diameter zircon (Cherniak & Watson, 2001). Zircons that crystallized at 1096 Ma and then lost $>$ 90% of their Pb at 1091.6 Ma could give apparent U-Pb dates of 1091.8 Ma (Supporting Information). However, CL imagery reveals sharp boundaries between zones of differing CL response (Supporting Information) on the scale of \sim 2 μm . Such CL zoning patterns are dominantly attributed to concentration variations in the rare earth element Dy (Remond et al., 1992). A time-temperature

497 history that results in 90% Pb diffusion out of a 120 μm diameter zircon would also cause
 498 Dy re-equilibration throughout a zircon, leaving no clear zonation. Therefore a scenario
 499 where the zircons first crystallized during Duluth Complex magmatism and subsequently
 500 lost more than 90% of Pb is difficult to reconcile with the preservation of such thin zona-
 501 tions.

502 Based on Sm-Nd isotopic data, Morrison et al. (1983) favored a scenario where the
 503 anorthosite cumulates became xenoliths at an age of 1.9 Ga. While a ca. 1096 Ma Du-
 504 luth Complex age is difficult to explain given the U-Pb dates, a ca. 1900 Ma age can-
 505 not be reconciled with the data. To reset the U-Pb date of the zircons to be 1091.8 Ma
 506 at an emplacement time of 1091.6 Ma (the minimum age of emplacement for the Silver
 507 Bay intrusion date, Fig. 4) would require diffusive loss of >99.95% of the Pb from the
 508 zircons (Supporting Information). More Pb retention in zircons will exhibit as signifi-
 509 cant discordant ages and be inconsistent with the geochronology data (Fig. 4). The Sm-
 510 Nd age of 1.9 Ga from the anorthosite xenoliths is more likely the result of contamina-
 511 tion by older crust. Isotopic studies of MCR felsic rocks by Vervoort et al. (2007) indi-
 512 cate that anatetic melts in the early MCR magmatic stage were largely generated from
 513 Early Proterozoic (\sim 2.1 Ga) crust. Because of assimilation and anatexis of the lower crust,
 514 the plagioclase cumulates where the anorthosite xenoliths originated could have recorded
 515 this contamination, which is eventually reflected in the older Sm-Nd isotopic signatures
 516 within the Beaver River anorthosite xenoliths discovered by Morrison et al. (1983).

517 An alternative scenario consistent with an older formation age of the anorthosites
 518 is if the zircons crystallized long after the plagioclase. This scenario would require that
 519 interstitial melt pockets from which zircons crystallized remained liquid within the pla-
 520 gioclase cumulate until they were entrained by the Beaver River diabase *ca.* 1092 Ma
 521 and cooled. The mantle plume related heat regime of the Yellowstone hotspot has led
 522 to modern Moho temperatures that can be $>800^\circ\text{C}$ (Schutt et al., 2018). If a similar heat
 523 regime occurred during the crystallization of the anorthositic mush of the Duluth Com-
 524 plex magmatism and was sustained for 4 million years, there is the potential for partial
 525 melt. However, it would be difficult for such melt to stay in place and not to diffuse out
 526 of the cumulate on these long timescales.

527 The geochemical evidence for the zircons being comagmatic with the plagioclase
 528 is difficult to reconcile with zircon crystallization significantly postdating anorthosite cu-

mulate formation. The presence of REE zonation is difficult to reconcile with scenarios where there is significant Pb diffusion that appreciably reset the U-Pb dates. It is likely that Beaver River diabase anorthosite xenoliths are entrained cumulate enclaves that formed at the time of Beaver Bay Complex magmatism. Regardless, the U-Pb date of 1091.83 ± 0.21 Ma from zircons in the anorthosite xenolith constrains the Beaver River diabase to have been emplaced after that date and before the 1091.61 ± 0.14 Ma date of the cross-cutting Silver Bay aplite intrusion (Fig. 4).

536 **4.2 A comagmatic relationship between the Beaver River diabase and 537 the Greenstone Flow**

538 Given the existence of many anorthosite xenoliths whose short-axis diameters of-
539 ten reach tens of meters and can be as wide as 180 meters (Fig. 1; Boerboom (2004);
540 Boerboom et al. (2006)), the Beaver River diabase magma conduits must have been at
541 least this wide during magma ascent. It would be consistent with such wide conduits ex-
542 tending to hypabyssal depths for magma that flowed through these conduits to have vented
543 to the surface.

544 The high volume and composite nature of the extrusive Greenstone Flow of the Portage
545 Lake Volcanics lead to a match for this large and composite feeder system. Doyle (2016)
546 proposed a comagmatic link between the Beaver River diabase and the Greenstone Flow.
547 Doyle (2016) discovered that both the intrusive Bearver River diabase and the Green-
548 stone Flow have indistinguishable primary compositions that followed similar differen-
549 tiation patterns. Doyle (2016) also highlighted the shared petrographic textures between
550 the ophitic Beaver River diabase and the ophitic Greenstone Flow, which features the
551 plagioclase laths clustering together and joining along their long crystallographic axes.
552 The fosterite content of the olivines and enstatite content of the pyroxenes in the Beaver
553 River diabase together with the Silver Bay intrusions, and the Greenstone Flow have over-
554 lapping compositions consistent with the same magma source (Fig. 8). The composition
555 of the plagioclase within the units further strengthens this interpretation. Although there
556 are no known multi-crystalline anorthosite xenoliths in the Greenstone Flow, plagioclase
557 megacrysts occur in the lava flow. Analyses of the anorthite content from plagioclase megacrysts
558 show very similar values between the Beaver River diabase and the Greenstone Flow basalt
559 (Fig. 8, Doyle (2016)). In both units, the plagioclase cores are more enriched in anor-
560 thite than the rim and the groundmass. These data provide evidence that the core of

561 the plagioclase megacrysts in the Greenstone Flow derived from a similar source with
 562 those in the Beaver River diabase and that the rims are later overgrowths. These min-
 563 eralogical similarities are consistent with the interpretation that the Beaver River dia-
 564 base and the Greenstone Flow have the same magma source.

565 The magmatic linkage between the Beaver River diabase and the Greenstone Flow
 566 inferred from comparable lithologies and geochemistry can be further evaluated using
 567 the paleomagnetic pole positions and radiometric dates from both units (Fig. 6, 4). The
 568 heat diffusion model of the cooling history of the anorthosite xenoliths within the dia-
 569 base suggests that the time it takes to cool the diabase and anorthosite from low-titanium
 570 titanomagnetite Curie temperature ($\sim 580^{\circ}\text{C}$) to their blocking temperatures ($\sim 500^{\circ}\text{C}$)
 571 is on the time scale of a few thousand years (Fig. 7). This time scale is close to the typ-
 572 ical 10^4 years which is considered to be sufficient for averaging out secular variations of
 573 the geomagnetic field. Fig. 6 shows the site mean paleomagnetic pole positions from all
 574 diabase and anorthosite sites in this study against the previously synthesized Lauren-
 575 tia APWP developed using an Euler pole inversion to chronostratigraphically constrained
 576 volcanic poles in present-day coordinates (Swanson-Hysell et al., 2019). The site-mean
 577 pole positions of the diabase and anorthosite overlap within uncertainty ellipses and the
 578 mean pole positions fall between the 1095 Ma and 1090 Ma pole path positions (Fig. 6),
 579 consistent with the geochronology results (Fig. 4). Further, the mean paleomagnetic pole
 580 position derived from the Greenstone Flow share a common mean with those of the Beaver
 581 River diabase and the anorthosite xenoliths, but none of these poles share a common mean
 582 with the mean pole derived from the Portage Lake Volcanics (Fig. 6; Swanson-Hysell et
 583 al. (2019)). This result suggests that the timescale over which the Beaver River diabase
 584 and the Greenstone Flow acquired their magnetization may be too short to fully aver-
 585 age out secular variation. In this case, the overlapping pole positions between the Beaver
 586 River diabase and the Greenstone Flow strengthens their temporal correlation even more
 587 (Fig. 6).

588 The U-Pb dates provide strong support for this hypothesis by revealing equivalent
 589 ages for the Beaver River diabase and the Greenstone Flow. The age of the Beaver River
 590 diabase is constrained to be between the $^{206}\text{Pb}/^{238}\text{U}$ dates of 1091.83 ± 0.21 Ma and 1091.61
 591 ± 0.14 Ma (Fig. 4) giving an age estimate of 1091.7 ± 0.2 Ma (95% CI). This age is in-
 592 distinguishable with the $^{206}\text{Pb}/^{238}\text{U}$ date of 1091.59 ± 0.27 Ma for the Greenstone Flow
 593 (Fig. 4). These chronological constraints are consistent with a comagmatic linkage be-

594 between the Beaver River diabase and the Silver Bay intrusions and the extrusive Green-
 595 stone Flow.

596 The Portage Lake Volcanics, including the Greenstone Flow, are interpreted to have
 597 erupted into the main central graben of the Midcontinent Rift during an interval of sig-
 598 nificant subsidence (Fig. 9; Miller and Chandler (1997); Cannon and Hinze (1992)). In
 599 contrast to the thick accumulation in the Portage Lake Volcanics, the Beaver Bay Com-
 600 plex has an erosional (and slightly angular) unconformity atop it that is then covered
 601 by the the younger Schroeder-Lutsen basalt (Fig. 1; Miller et al. (2001)). This relation-
 602 ship suggests that the Beaver River diabase was emplaced into a rift flank highland that
 603 experienced uplift during the active development of the central graben (Swanson-Hysell
 604 et al., 2019). Eruptions fed through the Beaver River diabase network could have emerged
 605 from the rift flank or flowed from the highland into main rift basin where it accumulated
 606 as the Greenstone Flow and associated Portage lake Volcanics (Fig. 9). Silver Bay in-
 607 trusions from chambers of differentiated staging magmas later intruded the Beaver River
 608 diabase and the Greenstone Flow, adding to the composite lithologies of the lava flow
 609 and further inflating its heterolithic zone (Fig. 9). If the Greenstone Flow indeed con-
 610 nects through the Lake Superior basin to NE Minnesota and the Beaver River diabase,
 611 the volume of $\sim 1650 \text{ km}^3$ estimated by Longo (1984) must be a minimum. The full vol-
 612 ume of the Greenstone Flow likely reaches $\sim 6000 \text{ km}^3$ (Doyle, 2016), rivaling the largest
 613 known lava flows on Earth (Fig. 2).

614 5 Conclusion

615 High-precision U-Pb dates, together with paleomagnetic data, support the hypoth-
 616 esis that the Beaver River diabase was a feeder system to the high-volume Greenstone
 617 Flow. This intrusive-extrusive linkage is further bolstered by the similar compositions
 618 of the units. The large anorthosite xenoliths within the Beaver River diabase require that
 619 conduits feeding the magma to the surface had widths that exceeded 150 meters. As a
 620 result, there was voluminous emplacement of magma into the shallow subsurface and erup-
 621 tion into the Midcontinent Rift basin *ca.* 1092.7 Ma at the end of the main stage of Mid-
 622 continent Rift magmatism.

623 **Acknowledgments**

624 This research was funded by NSF EAR-1847277 to N.L.S.-H. and an Institute on Lake
625 Superior Geology Student Research Fund grant to Y.Z. Permits for fieldwork and sam-
626 pling from the Minnesota Department of Natural Resources are gratefully acknowledged.
627 We thank James Pierce and Blake Hodgin for assistance in the field. We thank Stephen
628 Self for providing constructive comments regarding mafic lava flow volumes. We thank
629 John Grimsich and Tim Teague at UC Berkeley EPS department for their help with pet-
630 rographic sample preparation and analyses. Paleomagnetic data associated with this study
631 are available within the MagIC database (<https://earthref.org/MagIC/17089/26d9073f-2447-4f46-85fb-8596ce5b3aab>) and all data are within a Github repository associ-
632 ated with this work (https://github.com/Swanson-Hysell-Group/2021_AX_BD) that
633 is also archived on Zenodo (insert URL after revisions). This repository also contains
634 Python code related to calculations, visualizations and statistical tests discussed herein.
635

Table 1:
Summary of new site level paleomagnetic data for the Beaver River diabase and anorthosite xenoliths. n/N: number of samples/sites analyzed and included in the site/grand mean; dec_{is} & inc_{is} : in situ mean declination and inclination for the site; dec_{te} & inc_{te} : tilt-corrected mean declination and inclination for the site; k: Fisher precision parameter; R: resultant vector length; α_{95} : 95% confidence limit in degrees; VGP lat.—latitude of the virtual geomagnetic pole for the site; VGP lon—longitude of the virtual geomagnetic pole for the site. Full measurement level data are available within the MagIC database. <https://earthref.org/MagIC/17102/400e0fb3-a79b-42bd-aaeb-9005d2a3b488>.

site	lat	lon	n/N	dec_{is}	dec_{te}	inc_{is}	inc_{te}	k	α_{95}	VGP lat _{is}	VGP lon _{is}	VGP lat _{te}	VGP lon _{te}
AX1	47.2	-91.4	8.0	293.3	42.6	288.8	54.9	536.0	2.4	33.4	180.0	37.1	193.2
AX2	47.2	-91.4	9.0	282.0	31.3	277.4	42.6	145.0	4.3	20.4	181.8	22.6	191.1
AX3	47.6	-90.9	10.0	290.4	28.2	285.1	38.6	69.0	5.9	24.7	174.5	25.9	183.7
AX4	47.6	-90.9	7.0	291.9	20.0	288.3	30.7	91.0	6.4	22.3	169.8	24.4	177.2
AX5-10	47.6	-90.9	14.0	286.2	29.1	280.7	38.1	269.5	2.5	22.3	178.1	22.7	186.5
AX11	47.4	-91.2	8.0	284.9	23.5	281.7	35.2	305.0	3.2	19.1	176.3	22.0	184.1
AX12	47.3	-91.3	6.0	299.9	42.5	297.3	55.2	36.0	11.3	37.8	175.1	43.0	188.4
AX13	47.4	-91.2	9.0	289.8	23.0	287.3	35.1	434.0	2.5	22.2	172.4	25.7	180.0
AX14	47.3	-91.3	7.0	296.9	38.2	293.9	50.8	256.0	3.8	33.7	174.5	38.2	186.1
AX15	47.3	-91.3	8.0	282.9	42.3	275.8	53.5	86.0	6.0	26.2	187.2	27.9	199.8
AX16	47.3	-91.3	8.0	273.7	39.1	265.8	49.2	396.0	2.8	18.5	191.6	19.0	202.9
AX17	47.3	-91.3	8.0	273.6	49.8	261.6	59.6	647.0	2.2	24.3	198.3	23.7	213.5
AX18	47.3	-91.3	9.0	283.8	45.5	276.0	56.9	535.0	2.2	28.5	188.7	30.2	202.8
AX19	47.3	-91.3	8.0	293.9	35.8	290.7	48.2	65.0	2.1	30.5	175.4	34.6	186.0
AX20	47.3	-91.3	5.0	294.5	44.3	290.0	56.7	271.0	4.7	35.1	180.4	39.0	194.5
AX21	47.3	-91.3	8.0	301.7	37.7	301.7	50.5	803.0	2.0	36.7	170.4	42.1	181.7
AX22	47.4	-91.2	9.0	297.2	43.1	293.8	55.7	208.0	3.6	36.3	177.6	41.0	191.1
Anorthosite mean		17.0	289.3	36.5	284.5	48.2	55.0	4.9	28.0	179.6	30.9	190.8	
BD1	47.2	-91.4	15.0	293.1	40.9	288.8	53.2	623.0	1.5	32.4	179.0	36.1	191.6
BD2	47.6	-90.9	8.0	286.6	22.7	282.0	32.6	122.0	5.0	19.9	175.0	21.0	182.8
BD3	47.4	-91.2	8.0	286.6	29.8	282.8	41.6	212.0	3.8	22.9	177.9	25.8	186.9
BD4	47.3	-91.3	8.0	300.2	40.7	297.9	53.4	47.0	8.2	37.1	173.6	42.3	186.0
BD5	47.3	-91.3	8.0	282.7	44.8	274.8	56.0	271.0	3.4	27.4	188.9	28.9	202.6
BD6	47.3	-91.3	9.0	300.0	33.2	298.3	64.0	64.0	6.5	33.4	169.2	38.6	178.9
BD7	47.3	-91.3	7.0	292.4	53.1	285.0	65.3	305.0	3.5	38.5	189.2	41.3	208.3
BD8	47.2	-91.4	10.0	287.9	52.8	278.8	64.5	300.0	2.8	35.3	191.8	37.1	209.9
BD9	47.2	-91.3	7.0	278.2	33.8	272.3	44.6	55.0	8.2	19.0	185.7	20.4	195.6
BD10	47.4	-91.2	10.0	297.0	46.2	293.0	58.7	341.0	2.6	37.8	180.0	42.2	195.1
BD11	47.4	-91.3	8.0	296.4	41.7	293.0	54.2	429.0	2.7	35.1	177.1	39.5	189.9
BD12	47.3	-91.3	8.0	288.8	38.1	284.1	50.1	141.0	4.7	28.1	180.4	31.3	191.8
BD13	47.5	-91.1	8.0	280.4	22.4	276.9	33.6	341.0	3.0	15.6	179.2	18.0	186.7
BD15	47.7	-90.6	8.0	300.1	2.3	299.3	14.2	119.0	5.1	20.6	156.9	24.8	161.7
BD17	47.4	-91.2	8.0	295.1	28.5	292.9	41.0	550.0	2.4	28.0	170.8	32.3	179.3
Diabase mean		15.0	291.0	35.7	286.9	47.7	51.6	5.0	29.0	178.2	32.5	189.5	

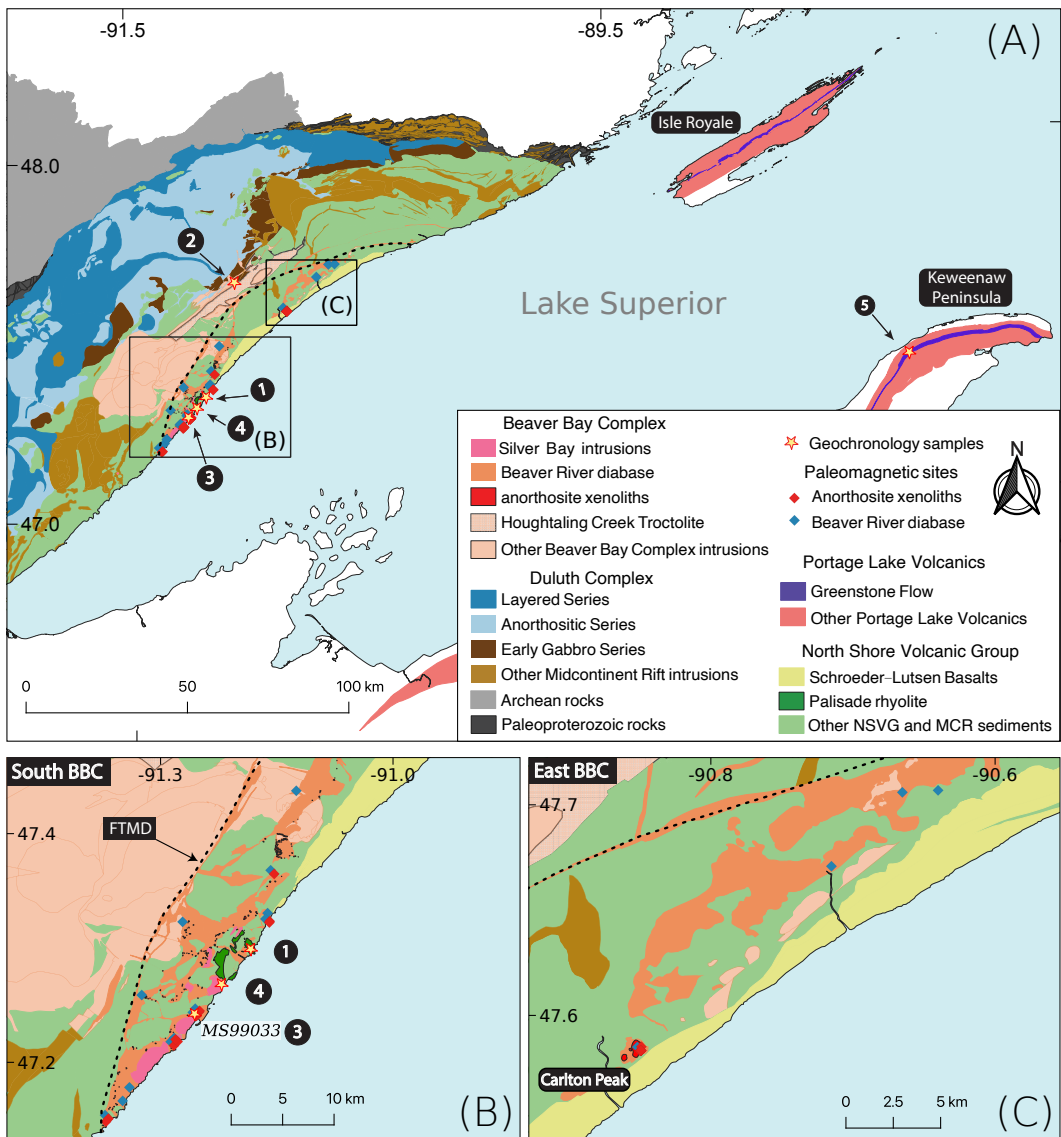


Figure 1: (A) Geologic map of exposures of Midcontinent Rift volcanics and intrusives in the western Lake Superior region. The Greenstone Flow (purple) of the Portage Lake Volcanics (red) outcrops throughout the Keweenaw Peninsula and Isle Royale. (B) Regional map of paleomagnetic and geochronologic sites in the southern Beaver Bay Complex (south BBC). Note that paleomagnetic site AX16 and geochronology sample MS99033 are from the same anorthosite xenolith. The geochronology sample numbers in (A) and (B) correspond to those in Fig. 4. (C) Regional map of paleomagnetic sites in the eastern Beaver Bay Complex (east BBC). The xenolith at Carlton Peak is >100 meters in diameter. The younger Schroeder-Lutsen basalt of the North Shore Volcanic Group (NSVG) is lying unconformably atop the Beaver River diabase and other NSVG units. The nomenclature of the “southern” and “eastern” Beaver Bay Complex follows Miller and Chandler (1997). FTMD - Finland tectonomagmatic discontinuity, traced out by the dashed black line. Bedrock geology is from Miller et al. (2001) and Jirsa et al. (2011).

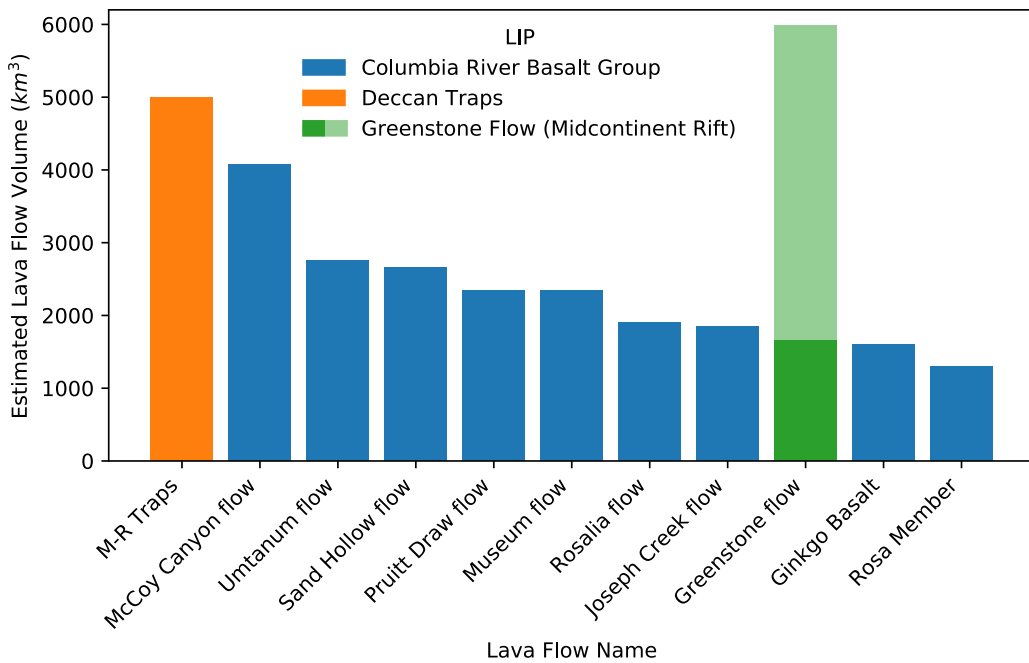


Figure 2: Bar plot of ten of the world's most voluminous single mafic lava flows currently known. With an estimated minimum volume of $\sim 1650 \text{ km}^3$ and likely volume as high as $\sim 6000 \text{ km}^3$, the Greenstone Flow from the 1.1 Ga Midcontinent Rift stands amongst the giant lava flows from the Deccan Traps and Columbia River basalts. M-R Traps = Mahabaleshwar–Rajahmundry lava flow in the Deccan Traps.

Volume estimates from Self et al. (2008), Bryan et al. (2010), Longo (1984), and Doyle (2016).

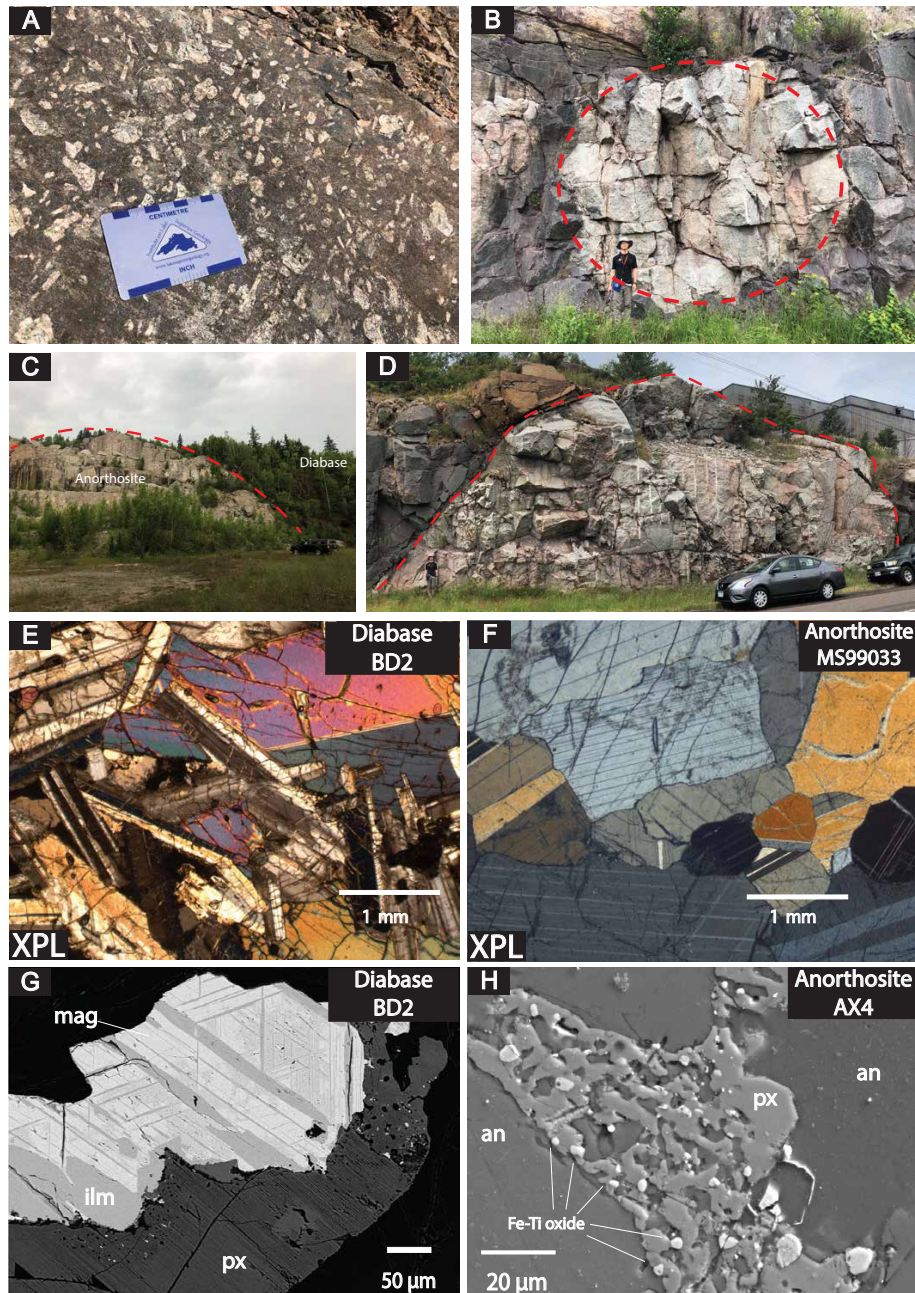


Figure 3: Field photographs and petrographic images of the Beaver River diabase and the anorthosite xenoliths within it. (A) Centimeter-sized plagioclase megacrysts in the diabase. (B) Rounded anorthosite xenolith with a diameter of ~ 7 meters fully entombed within the diabase. (C) Exposure of a giant Carlton Peak anorthosite with a diameter >100 m. (D) 27.5 m diameter anorthosite xenolith sampled as paleomagnetic site AX16 and geochronology sample MS99033. (E) Cross polarized (XPL) image of the subophitic texture of diabase at site BD2 (pyroxene partially enclosing plagioclase). (F) XPL image of anorthosite geochronology sample MS99033. Plagioclase crystals exhibit both granoblastic texture and interlocking lath fabrics. (G) Back scattered electron (BSE) image of a large Fe-Ti oxide with titanomagnetite-ilmenite lamellae in Beaver River diabase site BD2. (H) BSE image of micron-sized Fe-Ti oxides exsolved from pyroxene between plagioclase crystals in anorthosite xenolith site AX4.

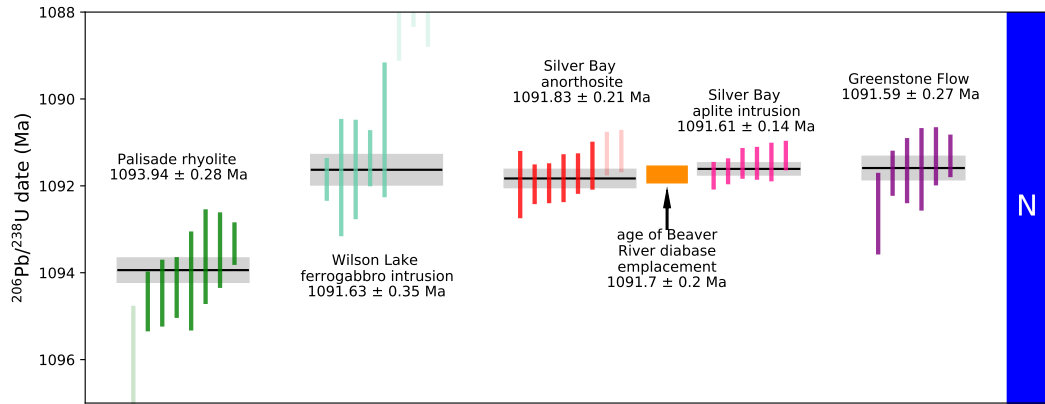


Figure 4: New $^{206}\text{Pb}/^{238}\text{U}$ zircon date of the anorthosite xenolith (dark orange) plotted in context of previously published $^{206}\text{Pb}/^{238}\text{U}$ zircon dates from the North Shore Volcanic Group (NSVG) and other Beaver Bay Complex intrusions (Swanson-Hysell et al., 2019, 2020). These high-precision dates are consistent with field observations that the Beaver River diabase crosscuts the Palisade rhyolite (dark green) and is cut by the Silver Bay intrusions (pink). The estimated age of the Beaver River diabase from these constraints is shown with an orange box the represented the 95% confidence interval. Each vertical bar corresponds to one $^{206}\text{Pb}/^{238}\text{U}$ date from a single zircon crystal. The translucent bars represents zircons with interpreted Pb loss and are therefore not included in the weighted mean age calculations. Horizontal lines and gray boxes represent weighted mean $^{206}\text{Pb}/^{238}\text{U}$ dates and their analytical uncertainty. The numbers of each geochronology sample corresponds to those in Fig. 1 where locations of these samples are shown.

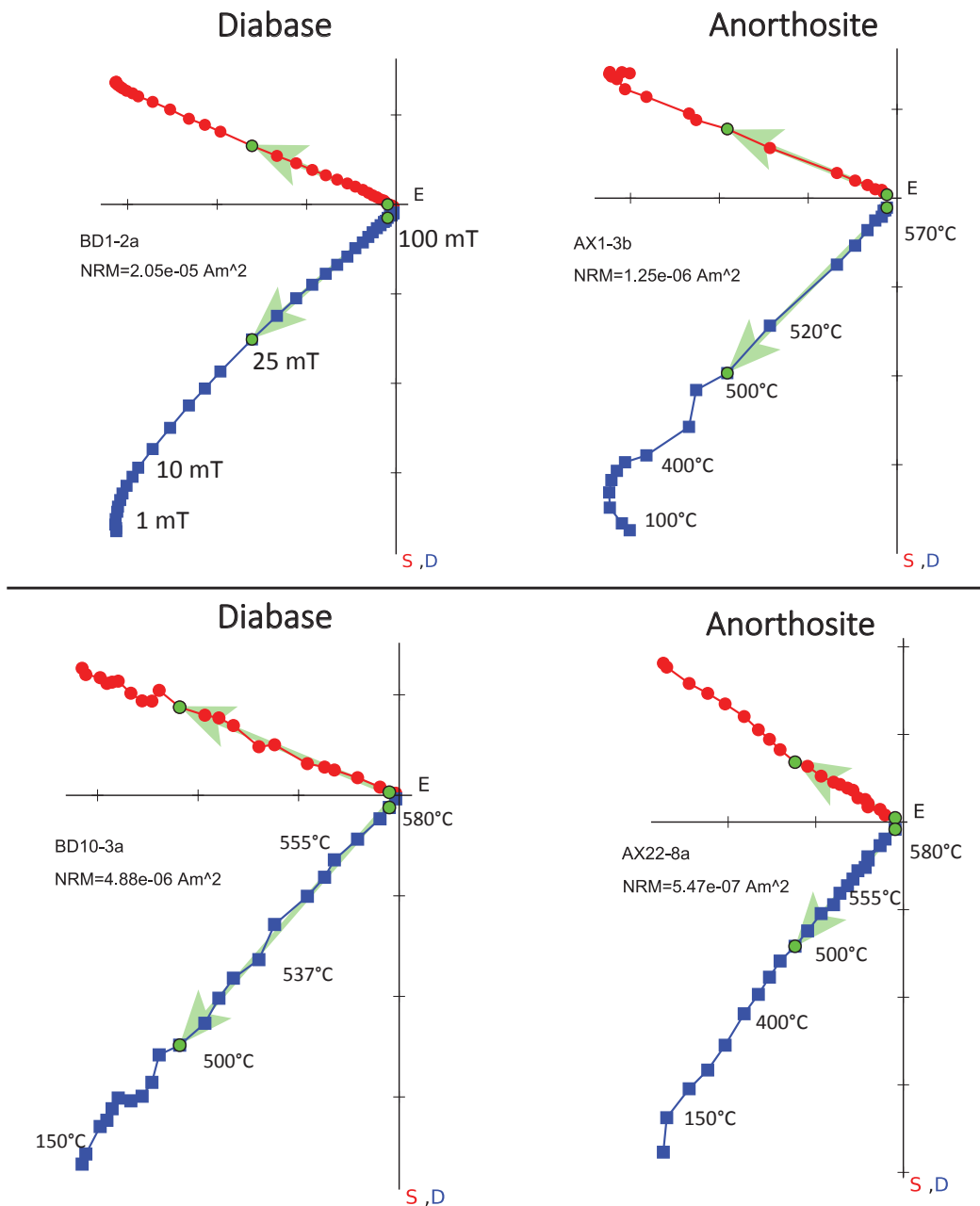


Figure 5: Example orthogonal vector demagnetization diagrams for diabase and anorthosite specimens. Anorthosite site AX1 is from a xenolith within the diabase sampled as BD1. Similarly, AX22 is from a xenolith with the BD10 diabase. Both AF and thermal demagnetization show dominantly univectoral decay of characteristic remanent magnetizations (ChRM) toward the origin after removal of minimal secondary components. The data reveal very similar ChRM directions between the paired diabase and anorthosite xenoliths sites.

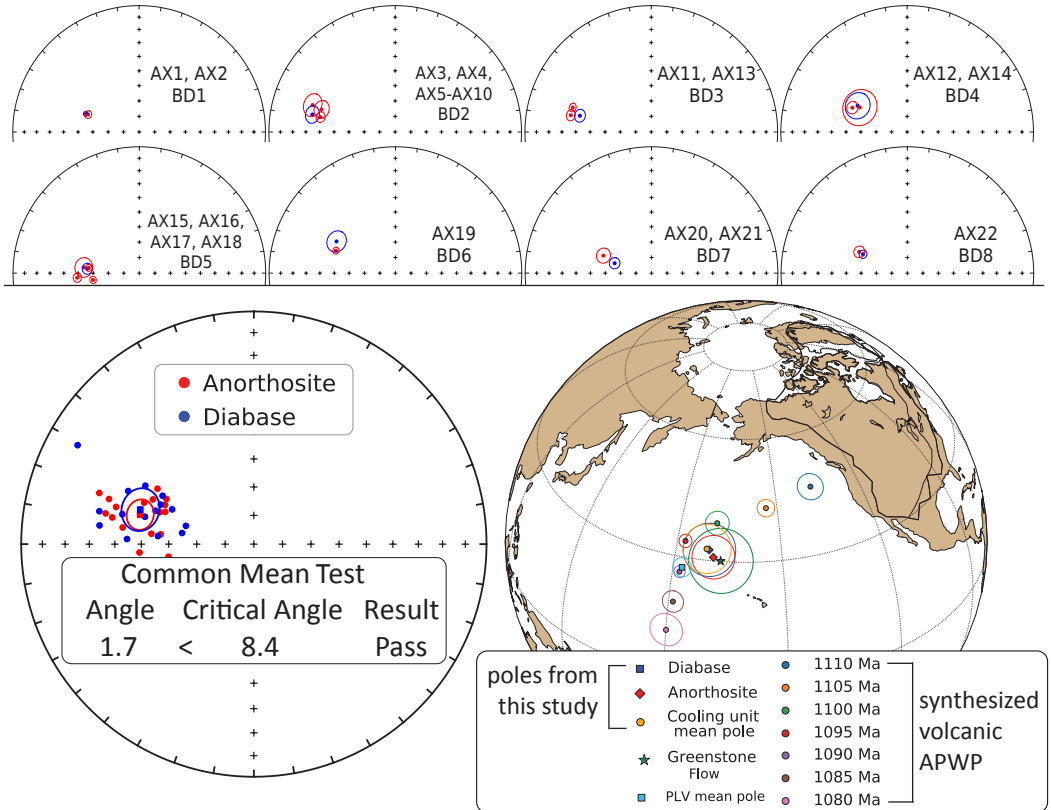


Figure 6: Top: Equal area plots of paleomagnetic directions from the anorthosite xenoliths and their local diabase hosts. AX: anorthosite xenolith site; BD: Beaver River diabase site. Bottom: Site mean paleomagnetic directions from the Beaver River diabase and anorthosite xenoliths are plotted on equal area plots. The anorthosite and diabase sites share a common mean as summarized by the results of the McFadden and McElhinny (1990) common mean test. Mean paleomagnetic pole positions of all diabase sites, all anorthosite sites, as well as a grand mean pole developed by grouping the anorthosite and diabase sites into individual cooling units are plotted against a synthesized Laurentia APWP based on poles from Midcontinent Rift volcanics and sedimentary rocks (Swanson-Hysell et al., 2019). The paleomagnetic poles from the diabase and anorthosite are indistinguishable with the Greenstone Flow pole developed by Foucher (2018), but they all are distinct from the Portage Lake Volcanics mean pole (Swanson-Hysell et al., 2019). All directions shown are tilt corrected.

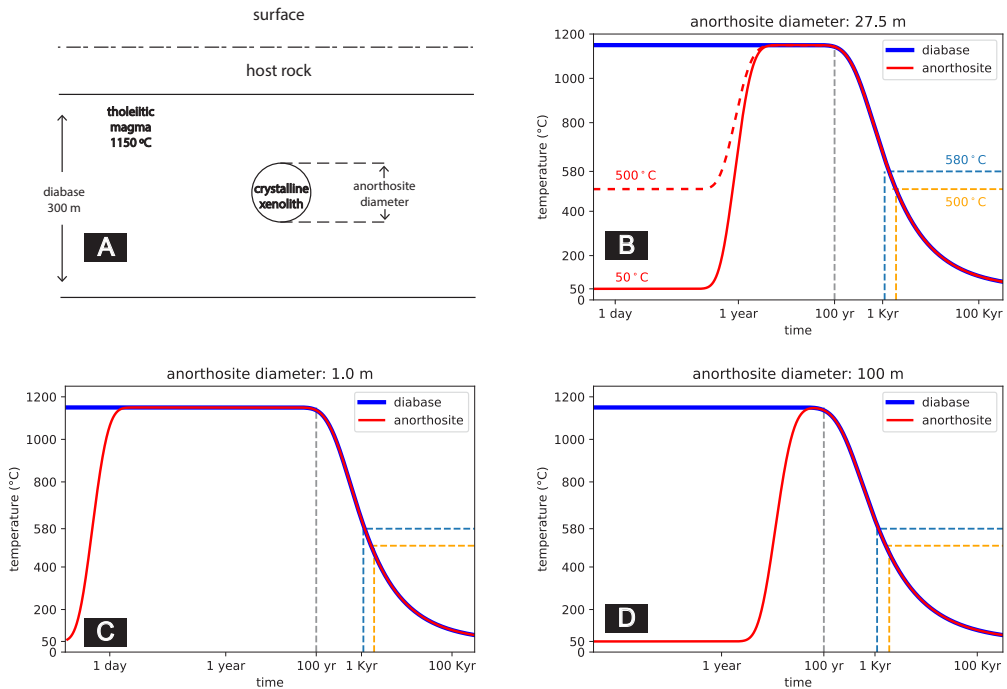


Figure 7: Thermal history model of the Beaver River diabase and its anorthosite xenoliths after emplacement at hypabyssal depths. (A) Schematic diagram for the thermal model considering cool anorthosite xenoliths as crystalline spheres residing in the middle of a diabase sill. Together they are hosted by cool country rocks at shallow depths. (B) Specific model for anorthosite AX16 (diameter of 27.5 meters) within its diabase sill host which is estimated to be 323 meters thick. (C) Thermal history model considering an anorthosite xenolith 1 meter in diameter residing in a 300 meter diabase sill. (D) Thermal history model considering an anorthosite xenolith 100 meter in diameter residing in a 300 meter diabase sill. These models show that anorthosite xenoliths were heated up to the diabase melt temperature after the emplacement, regardless of size. The time elapsed between at magnetite blocking temperatures (580°C and 500°C) during cooling is on the scale of a thousand years.

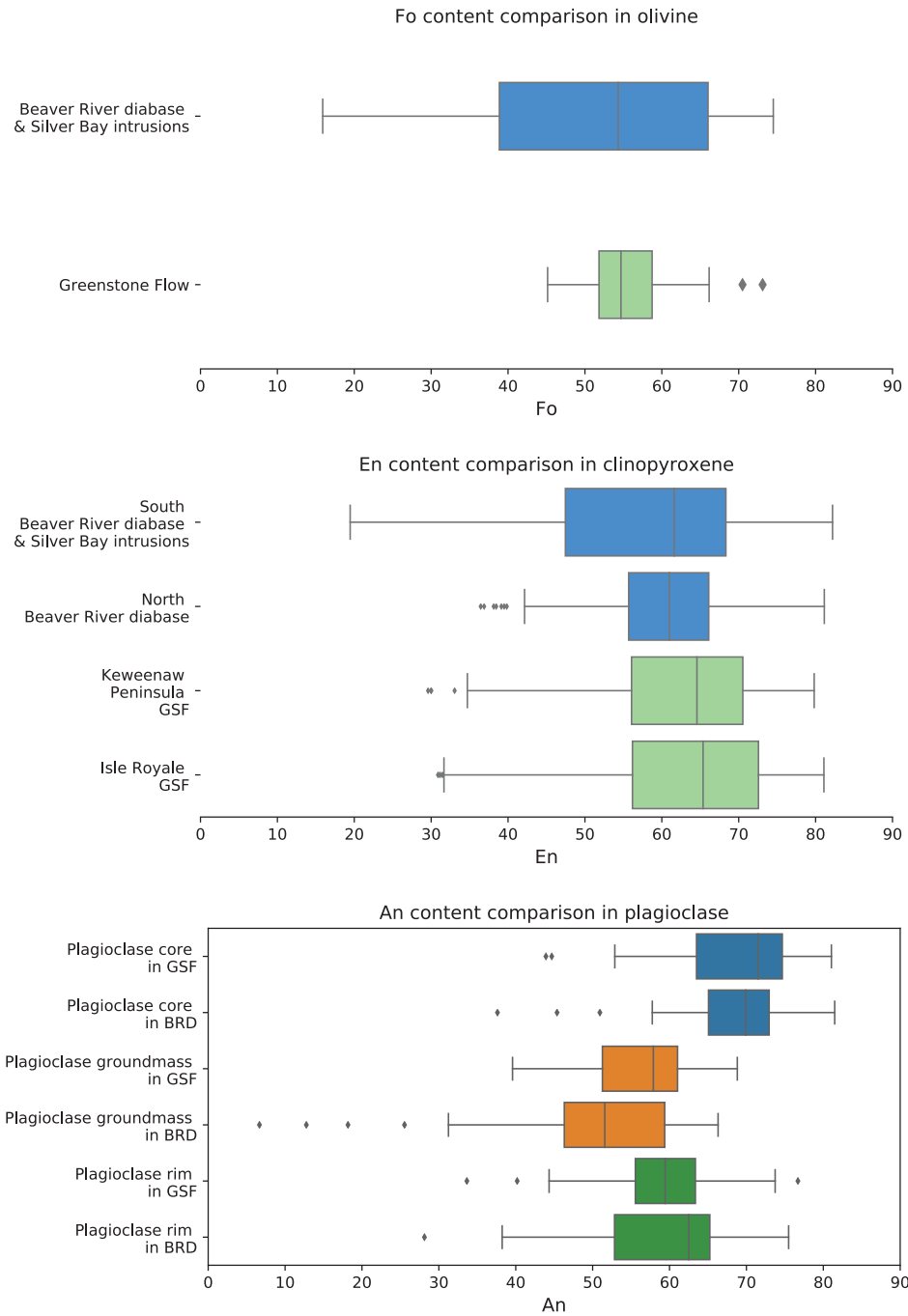


Figure 8: Box plots of geochemical analyses of olivine, pyroxene, and plagioclase in the Beaver River diabase (BRD) and Greenstone Flow (GSF). The fosterite content in olivine crystals and the enstatite content in clinopyroxene crystals are very similar in the Beaver River diabase and the Greenstone Flow. The anorthite concentrations in the core, groundmass, and rim of the plagioclase megacrysts within the Beaver River diabase and the Greenstone Flow share very similar patterns and the distributions are nearly identical. The box encloses the middle 50% of the data ranges (i.e., the interquartile range), and the notch represents the median values. The whiskers extend to the 2.5th and 97.5th percentile values. Fo-fosterite; En-enstatite; An-anorthite. Data from Doyle (2016).

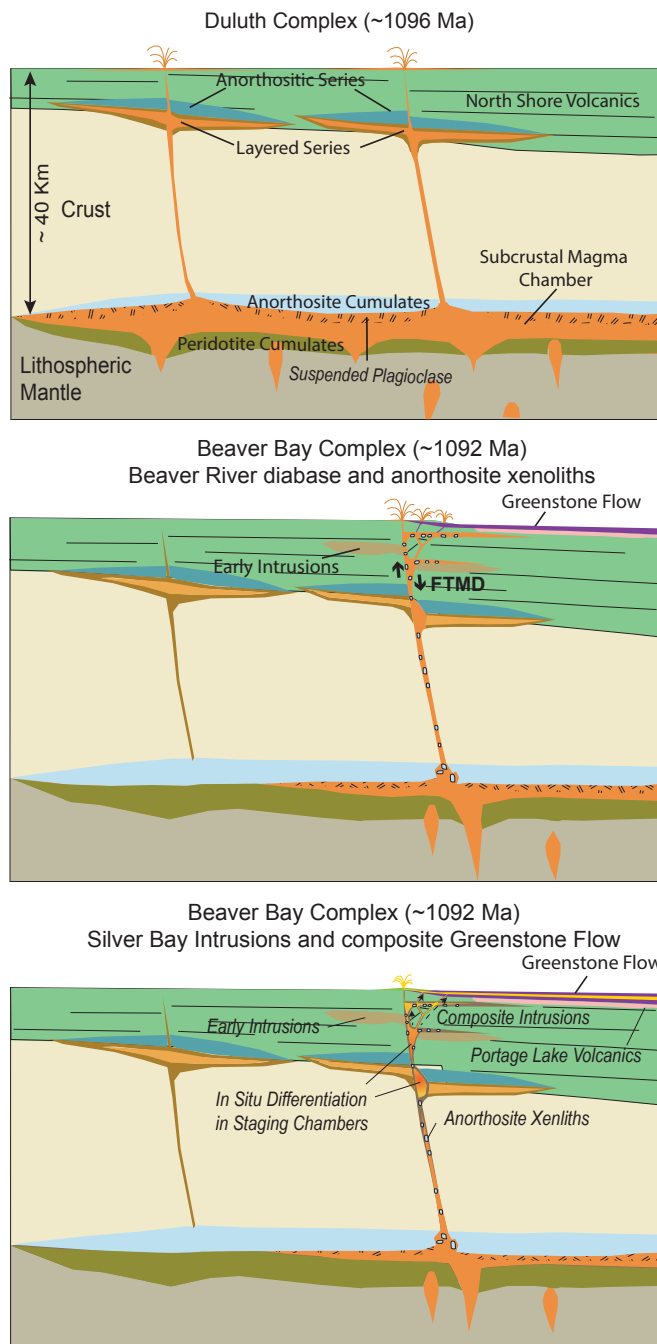


Figure 9: Schematic model for the emplacement of the *ca.* 1096 Ma Duluth Complex, the *ca.* 1092 Ma Beaver Bay Complex, Greenstone Flow and associated anorthositic lithologies. Top: Duluth Complex Anorthositic Series formed by subhorizontal emplacement of plagioclase crystal mushes generated by plagioclase flotation in subcrustal magma chambers. The Layered Series formed by emplacement of crystal-poor mafic magmas beneath the Anorthositic Series and variable differentiation by in situ fractional crystallization. Middle: Intrusion of the anorthosite xenolith-bearing Beaver River diabase of the Beaver Bay Complex along a major crustal fault (FTMD-Finland Tectonomagmatic Discontinuity) and its massive eruption at surface to form the Greenstone Flow. Bottom: Emplacement of the composite Beaver River diabase and Silver Bay intrusions into the diabase and the Greenstone Flow were generated by differentiation in deeper staging chambers. The ⁻³¹⁻ erosional unconformity between the Schroeder-Lutsen basalt and the Beaver River diabase suggest the diabase was emplaced into an uplifted rift flank highland, allowing for flank eruptions of the Greenstone Flow into the main Midcontinent Rift basin.

636 **References**

- 637 Beck, M. E. (1970). Paleomagnetism of Keweenawan Intrusive Rocks, Min-
 nesota. *Journal of Geophysical Research*, 75(26), 4985–4996. doi:
 638 10.1029/jb075i026p04985
- 640 Beck, M. E., & Lindsley, N. C. (1969). Paleomagnetism of the Beaver Bay Complex,
 641 Minnesota. *Journal of Geophysical Research*, 74(8), 2002–2013. doi: 10.1029/
 642 jb074i008p02002
- 643 Boerboom, T. J. (2004). *M-147 Bedrock geology of the Split Rock Point quadrangle,*
 644 *Lake County, Minnesota* (Tech. Rep.). Minnesota Geological Survey.
- 645 Boerboom, T. J., Green, J., & Albers, P. (2007). *M-174 Bedrock geology of the Lut-*
 646 *sen quadrangle, Cook County, Minnesota* (Tech. Rep.). Minnesota Geological
 647 Survey.
- 648 Boerboom, T. J., & Green, J. C. (2006). *M-170 Bedrock geology of the Schroeder*
 649 *quadrangle, Cook County, Minnesota* (Tech. Rep.). Minnesota Geological Sur-
 650 vey.
- 651 Boerboom, T. J., Green, J. C., Albers, P., & Miller, J., J.D. (2006). *M-171 Bedrock*
 652 *geology of the Tofte quadrangle, Cook County, Minnesota* (Tech. Rep.). Min-
 653 nesota Geological Survey.
- 654 Books, K. G., White, W. S., & Beck, M. E. (1966). *Magnetization of Keweenawan*
 655 *gabbro in northern Wisconsin and its relation to time of intrusion.* Geological
 656 Survey Research.
- 657 Bryan, S. E., Peate, I. U., Peate, D. W., Self, S., Jerram, D. A., Mawby, M. R., ...
 658 Miller, J. A. (2010). The largest volcanic eruptions on Earth. *Earth-Science*
 659 *Reviews*, 102(3-4), 207–229. doi: 10.1016/j.earscirev.2010.07.001
- 660 Cannon, W. F., & Hinze, W. J. (1992). Speculations on the origin of the North
 661 American Midcontinent rift. *Tectonophysics*, 213(1-2), 49–55. doi: 10.1016/
 662 0040-1951(92)90251-z
- 663 Cannon, W. F., & Nicholson, S. W. (2001). Geologic map of the Keweenaw Penin-
 664 sula and adjacent area, Michigan. *USGS Numbered Series*, 2696.
- 665 Cherniak, D., & Watson, E. (2001). Pb diffusion in zircon. *Chemical Geology*, 172(1-
 666 2), 5–24. doi: 10.1016/s0009-2541(00)00233-3
- 667 Condon, D. J., Schoene, B., McLean, N. M., Bowring, S. A., & Parrish, R. R. (2015,
 668 9 1). Metrology and traceability of U-Pb isotope dilution geochronology

- 669 (EARTHTIME tracer calibration part I). *Geochimica et Cosmochimica Acta*,
670 *164*, 464–480. doi: 10.1016/j.gca.2015.05.026
- 671 Davis, D. W., & Paces, J. B. (1990). Time resolution of geologic events on the
672 Keweenaw Peninsula and implications for development of the Midcontinent
673 Rift system. *Earth and Planetary Science Letters*, *97*(1-2), 54–64. doi:
674 10.1016/0012-821x(90)90098-i
- 675 Delaney, P. (1987). *Heat transfer during emplacement and cooling of mafic dykes*.
676 Geological Association of Canada.
- 677 Doyle, M. (2016). *Geologic and geochemical attributes of the Beaver River Diabase*
678 *and Greenstone Flow: Testing a possible intrusive-volcanic link in the 1.1 Ga*
679 *Midcontinent Rift* (Unpublished master's thesis). University of Minnesota.
- 680 Fairchild, L. M., Swanson-Hysell, N. L., Ramezani, J., Sprain, C. J., & Bowring,
681 S. A. (2017). The end of Midcontinent Rift magmatism and the paleogeogra-
682 phy of Laurentia. *Lithosphere*, *9*(1), 117–133. doi: 10.1130/l580.1
- 683 Ferry, J. M., & Watson, E. B. (2007). New thermodynamic models and revised cal-
684ibrations for the Ti-in-zircon and Zr-in-rutile thermometers. *Contributions to*
685 *Mineralogy and Petrology*, *154*(4), 429–437. doi: 10.1007/s00410-007-0201-0
- 686 Foucher, M. (2018). *Probing the Precambrian geodynamo: analysis of the geomag-*
687 *netic field behavior and calibration of pseudo-thellier paleointensity method for*
688 *Mesoproterozoic rocks* (Unpublished doctoral dissertation). Michigan Techno-
689 logical University.
- 690 Green, J. C. (1982). 5: Geology of Keweenawan extrusive rocks. *Geological Society*
691 *of America Memoirs*, *156*, 47–56.
- 692 Grout, S. G. M., Frank F. (1939). The geology of the anorthosites of the Minnesota
693 coast of Lake Superior. Minnesota Geological Survey.
- 694 Heaman, L. M., Easton, R. M., Hart, T. R., Hollings, P., MacDonald, C. A., &
695 Smyk, M. (2007). Further refinement to the timing of Mesoproterozoic mag-
696 matism, Lake Nipigon region, Ontario. *Canadian Journal of Earth Sciences*,
697 *44*(8), 1055–1086. doi: 10.1139/e06-117
- 698 Hinze, W. J., & Chandler, V. W. (2020). Reviewing the configuration and extent
699 of the Midcontinent Rift system. *Precambrian Research*, *342*, 105688. doi: 10
700 .1016/j.precamres.2020.105688
- 701 Huber, N. (1973). *The Portage Lake Volcanics (Middle Keweenawan) on Isle*

- Ga Midcontinent Rift in the Lake Superior Region – An Overview. In *Field guide to the copper-nickel-platinum group element deposits of the lake superior region*. Precambrian Research Center.

Miller, J., J.D., Severson, M. J., Chandler, V. W., & Peterson, D. M. (2001). *M-119 Geologic map of the Duluth Complex and related rocks, northeastern Minnesota* (Tech. Rep.). Minnesota Geological Survey.

Miller, J., J.D., & Weiblen, P. W. (1990). Anorthositic rocks of the Duluth Complex: Examples of rocks formed from plagioclase crystal mush. *Journal of Petrology*, 31(2), 295–339. doi: 10.1093/petrology/31.2.295

Morrison, D. A., Ashwal, L. D., Phinney, W. C., Shih, C.-Y., & Wooden, J. L. (1983). Pre-Keweenawan anorthosite inclusions in the Keweenawan Beaver Bay and Duluth Complexes, northeastern Minnesota. *Geological Society of America Bulletin*, 94(2), 206. doi: 10.1130/0016-7606(1983)94<206:paiitk>2.0.co;2

Paces, J. B., & Miller, J., J.D. (1993). Precise U-Pb ages of Duluth Complex and related mafic intrusions, northeastern Minnesota: Geochronological insights to physical, petrogenetic, paleomagnetic, and tectonomagmatic processes associated with the 1.1 Ga Midcontinent Rift System. *Journal of Geophysical Research: Solid Earth*, 98(B8), 13997–14013. doi: 10.1029/93jb01159

Remond, G., Cesbron, F., Chapoulie, R., Ohnenstetter, D., Roques-Carmes, C., & Schvoerer, M. (1992). Cathodoluminescence applied to the microcharacterization of mineral materials: a present status in experimentation and interpretation. *Scanning microscopy*, 6(1), 2.

Rubatto, D. (2002). Zircon trace element geochemistry: partitioning with garnet and the link between U–Pb ages and metamorphism. *Chemical Geology*, 184(1-2), 123–138. doi: 10.1016/s0009-2541(01)00355-2

Schaltegger, U., Fanning, C. M., Günther, D., Maurin, J. C., Schulmann, K., & Gebauer, D. (1999). Growth, annealing and recrystallization of zircon and preservation of monazite in high-grade metamorphism: conventional and in-situ U-Pb isotope, cathodoluminescence and microchemical evidence. *Contributions to Mineralogy and Petrology*, 134(2-3), 186–201. doi: 10.1007/s004100050478

Schoene, B., Crowley, J. L., Condon, D. J., Schmitz, M. D., & Bowring, S. A. (2006). Reassessing the uranium decay constants for geochronology using

- 768 ID-TIMS U–Pb data. *Geochimica et Cosmochimica Acta*, 70(2), 426–445. doi:
769 10.1016/j.gca.2005.09.007
- 770 Schutt, D. L., Lowry, A. R., & Buehler, J. S. (2018). Moho temperature and mobil-
771 ity of lower crust in the western United States. *Geology*, 46(3), 219–222. doi:
772 10.1130/g39507.1
- 773 Self, S., Jay, A., Widdowson, M., & Keszthelyi, L. (2008). Correlation of the Deccan
774 and Rajahmundry Trap lavas: Are these the longest and largest lava flows on
775 Earth? *Journal of Volcanology and Geothermal Research*, 172(1-2), 3–19. doi:
776 10.1016/j.jvolgeores.2006.11.012
- 777 Shank, S. G. (1989). The petrology of the Beaver Bay Complex near Silver Bay,
778 northeastern Minnesota. *Minnesota, University of Minnesota*.
- 779 Swanson-Hysell, N. L., Hoaglund, S. A., Crowley, J. L., Schmitz, M. D., Zhang,
780 Y., & Miller, J. D. (2020). Rapid emplacement of massive Duluth Com-
781 plex intrusions within the North American Midcontinent Rift. *Geology*. doi:
782 10.1130/g47873.1
- 783 Swanson-Hysell, N. L., Maloof, A. C., Weiss, B. P., & Evans, D. A. D. (2009).
784 No asymmetry in geomagnetic reversals recorded by 1.1-billion-year-old Ke-
785 weenawan basalts. *Nature Geoscience*, 2(10), 713–717. doi: 10.1038/ngeo622
- 786 Swanson-Hysell, N. L., Ramezani, J., Fairchild, L. M., & Rose, I. R. (2019). Failed
787 rifting and fast drifting: Midcontinent Rift development, Laurentia’s rapid mo-
788 tion and the driver of Grenvillian orogenesis. *GSA Bulletin*, 131(5-6), 913–940.
789 doi: 10.1130/b31944.1
- 790 Tauxe, L., Shaar, R., Jonestrask, L., Swanson-Hysell, N. L., Minnett, R., Koppers,
791 A. A. P., . . . Fairchild, L. (2016). PmagPy: Software package for paleomag-
792 netic data analysis and a bridge to the Magnetics Information Consortium
793 (MagIC) Database. *Geochemistry, Geophysics, Geosystems*, 17(6), 2450–2463.
794 doi: 10.1002/2016gc006307
- 795 Unsworth, J., & Duarte, F. J. (1979). Heat diffusion in a solid sphere and Fourier
796 theory: An elementary practical example. *American Journal of Physics*,
797 47(11), 981–983. doi: 10.1119/1.11601
- 798 van Hinsbergen, D. J. J., Steinberger, B., Doubrovine, P. V., & Gassmöller, R.
799 (2011). Acceleration and deceleration of India-Asia convergence since the
800 Cretaceous: Roles of mantle plumes and continental collision. *Journal of*

- 801 *Geophysical Research*, 116(B6). doi: 10.1029/2010jb008051
- 802 Vervoort, J. D., Wirth, K., Kennedy, B., Sandland, T., & Harpp, K. S. (2007). The
803 magmatic evolution of the Midcontinent rift: New geochronologic and geo-
804 chemical evidence from felsic magmatism. *Precambrian Research*, 157(1-4),
805 235–268. doi: 10.1016/j.precamres.2007.02.019
- 806 White, W. (1960). The Keweenawan lavas of Lake Superior, an example of flood
807 basalts. *American Journal of Science*, 258, 367–374.